

Processing aortic and pulmonary artery waveforms to derive the ventricle time-varying elastance

David J. Stevenson* Christopher E. Hann*
Geoffrey J. Chase* James Revie* Geoffrey M. Shaw**
Thomas Desaive*** Bernard Lambermont***
Alexandre Ghuyssen*** Phillippe Kolh***
Stefan Heldmann****

* *Department of Mechanical Engineering, University of Canterbury, Christchurch, New Zealand*

** *Department of Intensive Care, Christchurch Hospital, Christchurch, New Zealand*

*** *Hemodynamics Research Laboratory, University of Liege, Belgium*

**** *Department of Mechanical Engineering, TU Darmstadt, Germany*

Abstract: Time-varying elastance of the ventricles is an important metric both clinically and as an input for a previously developed cardiovascular model. However, currently time-varying elastance is not normally available in an Intensive Care Unit (ICU) setting, as it is an invasive and ethically challenging metric to measure. A previous paper developed a method to map less invasive metrics to the driver function, enabling an estimate to be achieved without invasive measurements. This method requires reliable and accurate processing of the aortic and pulmonary artery pressure waveforms to locate the specific points that are required to estimate the driver function. This paper details the method by which these waveforms are processed, using a data set of five pigs induced with pulmonary embolism, and five pigs induced with septic shock (with haemofiltration), adding up to 88 waveforms (for each of aortic and pulmonary artery pressure), and 616 points in total to locate. 98.2% of all points were located to within 1% of their true value, 0.81% were between 1% and 5%, 0.65% were between 5% and 10%, the remaining 0.32% were below 20%.

Keywords: Cardiovascular system, Time-varying elastance, Model-based cardiac diagnosis, Pressure waveform, Signal Processing, Intensive Care Unit, Porcine model

1. INTRODUCTION

In the Intensive Care Unit (ICU), cardiac disturbances are very difficult to diagnose and treat, which can lead to poor management of the circulation (Guyton and Hall (2000); Grenvik et al. (1989)). Left and right pressure-volume (PV) loops contain a large amount of information on cardiac function including all the states of filling, contraction, ejection and relaxation. From this data a cardiac elastance can be defined:

$$el(t) = \frac{P_{lv}(t)}{V_{lv}(t) - V_d} \quad (1)$$

where

$$\begin{aligned} V_d &\equiv \text{intercept of the end-systolic PV} \\ &\quad \text{relation with the volume axis} \\ P_{lv}(t) &\equiv \text{left ventricle pressure} \\ V_{lv}(t) &\equiv \text{left ventricle volume} \end{aligned} \quad (2)$$

Derived by Suga and Sagawa (1974), it is commonly called time varying elastance, and provides a load-independent measure of heart function (Oommen et al. (2003); Suga et al. (1973); Senzaki et al. (1996)), while representing the cardiac muscle activation. Time varying elastance is

typically normalised to one, and the resulting shape can be used as the input or driver function into lumped parameter models of the cardiovascular system (Smith et al. (2004)). The shape of the driver function thus approximates the change in cardiac muscle activation over time, and implicitly contains information on the ventricle pressure and volume profiles. However, determining the parameter V_d requires an invasive vena cava occlusion manoeuvre, and the left and right ventricle pressures and volumes, which is invasive and ethically challenging to measure. Hence, they are not available as typical ICU care.

Stevenson et al. (2010) developed a method to estimate the ventricle driver functions, based on pre-calculated, global correlations between the ventricle driver functions and less invasive measurements of the pulmonary artery and aortic pressure waveforms. These driver functions then provide the input into a previously developed eight chamber cardiovascular system (CVS) model (Starfinger et al. (2008)), as well as significant diagnostic information in relation to cardiac energetics. Hence, these estimates based on readily available data can have significant clinical potential.

The pre-calculated correlations map specific points on the aortic and pulmonary artery pressure waveforms to specific points on the driver function. The points on the driver function were chosen as a minimum set of points through which a smooth curve can be generated that captures the necessary dynamics of the actual driver function waveform. The locations on the pressure waveforms that map to the driver functions were found from known physiological connections and empirical relations (Stevenson et al. (2010)). They are shown briefly, without explanation, in Table 1 and Figures 1 and 2. This paper focus on the method of processing the pressure waveforms in order to locate the points required by the correlations, thus enabling these driver function estimates.

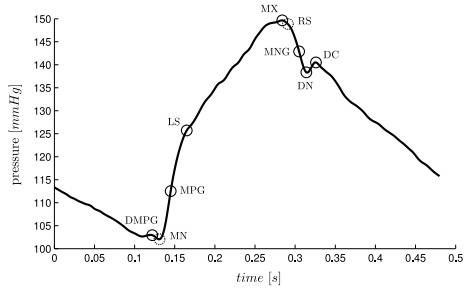


Fig. 1. Aortic pressure over one heart beat, including relevant points defined in Table 1, note that RS & MN are used only in locating other points

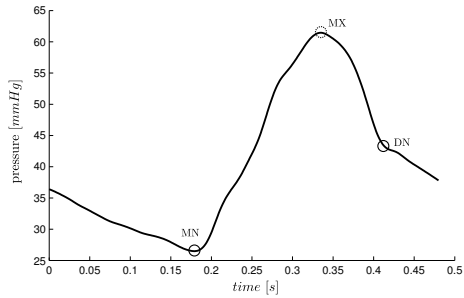


Fig. 2. Pulmonary artery pressure over one heart beat, including relevant points defined in Table 1, note that MX is used only as part of locating DN

2. CONCEPT

The concept behind this paper involves creating a set of correlations that map the less invasive metrics to the desired, more invasive metrics, where the correlations are later used to estimate the more invasive metrics. In this case, the correlation map aortic pressure, pulmonary artery pressure and global end diastolic volume to left and right ventricle time-varying elastance.

An illustration of this concept is given in Figure 3, while Figure 4 shows a more detailed picture. The process requires the pre-calculation of the correlations. To do this took a set of both the invasive and less invasive metrics must be available. From this set, correlations can be derived from known physiological connections, and empirically by lining up the two waveforms. To derive the empirical correlations, and (later) estimate the invasive metrics, a method for processing the waveforms must be developed. This method must be able to reliably and

accurately identify specific locations on these waveforms. This paper details that method.

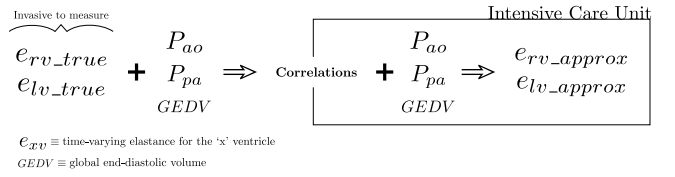


Fig. 3. The concept of estimating an invasive metric using pre-calculated, global correlations

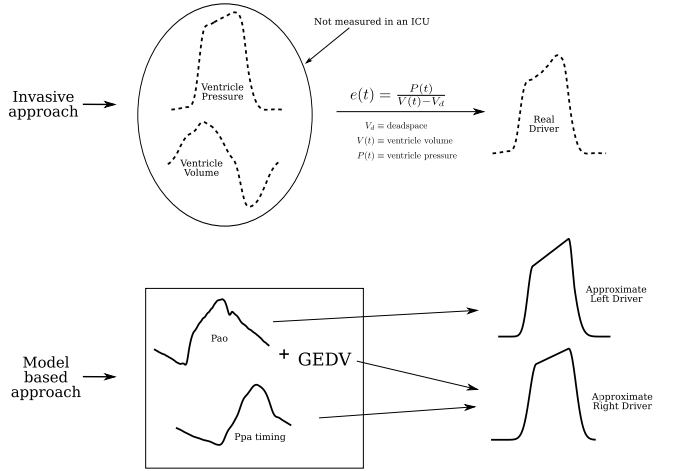


Fig. 4. Pictorial overview of the process of finding the real and approximate driver functions

3. METHODOLOGY

To enable driver function identification and its clinical outcomes, two pressure waveforms are processed to extract specific points of time, value and gradient. These waveforms are the aortic pressure (P_{ao}) and pulmonary artery pressure (P_{pa}). The accuracy and robustness of this processing is critical to the accuracy of the time-varying elastances built from the resulting data. A naming convention for these points of interest is defined in Table 1, and graphically in Figures 1-2 (Stevenson et al. (2010)).

Table 1. Naming convention

Left	Right	Description
el	er	driver function
P_{ao}	P_{ao}	aortic pressure
P_{pa}	P_{pa}	pulmonary artery pressure
$DMPG$		driver maximum positive gradient
MN	MN	minimum point
MPG		maximum positive gradient
LS		left shoulder
MX	MX	maximum point
RS		right shoulder
MNG		maximum negative gradient
DN	DN	dicotic notch
DC		dicotic crest
$t_{a,b}$	$t_{a,b}$	time of point b on waveform a

The processing method is described using P_{ao} as the pressure waveform. However, the same approach is used for P_{pa} , except where stated.

The points of interest, shown in Figures 1-2, are located in the following order, MX , MN , $DMPG$, LS , MPG , DN ,

RS , and DC , where previously located points are used in the location of subsequent points.

Note that before processing P_{ao} and P_{pa} , both waveforms were smoothed using a locally weighted 2nd degree polynomial regression (loess) over a range of 0.04 seconds.

3.1 Shear Transformation

To facilitate the extraction of a number of points, a shear transformation is defined:

$$(t, X(t)) \rightarrow (t, \phi_{shear}(X(t))) \quad (3)$$

$$\phi_{shear}(X(t)) = X(t) + mt + c, \quad t_0 < t < t_{end}$$

The parameters t_0 and t_{end} are set depending on the region of interest. The parameters m and c are chosen such that $\phi_{shear}(X(t_0)) = X(t_0)$ and $\phi_{shear}(X(t_{end})) = X(t_0)$ which leads to the following equations:

$$X(t_0) + mt_0 + c = X(t_0) \quad (4a)$$

$$X(t_{end}) + mt_{end} + c = X(t_0) \quad (4b)$$

Solving(4a) and(4b) yields:

$$m = \frac{X(t_0) - X(t_{end})}{t_{end} - t_0} \quad (5)$$

$$c = \frac{t_0(X(t_0) - X(t_{end}))}{t_{end} - t_0}$$

To better visualize this transformation, imagine a line from MN to MX (of Figure 1), rotated about MN so that this line is horizontal, while the time remains unchanged, e.g. a rotation and contraction that projects the line onto a horizontal surface (time). The effect of this transformation is to transform the point LS into a peak of a curve, and thus easier to locate. Figure 5 shows an example of this transformation. This shear transformation is applied to several regions to locate shoulders and changes of slope.

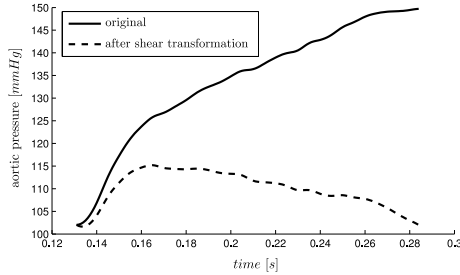


Fig. 5. the section from Figure 1 between MN and MX , before and after the shear transformation from(3).

3.2 MX , MN , and $DMPG$

MX is straight forward to locate as it is the global maximum of the waveform, the time of which is defined:

$$t_{MX} \equiv \text{time of maximum } P_{ao} \quad (6)$$

MN and $DMPG$ occur in close proximity around the global minimum of the pressure waveform. MN is thought of as the minimum of the pressure. However, it is not always the global minimum as in some cases there exists a trough just before $DMPG$ that is lower, and occasionally there exists a lower point in the second half of the waveform. Hence, it would be unreliable to locate MN as the global minimum.

Instead, a second property of MN is used, MN is located at the bottom of the steeply rising section from MN to LS , and MN always appears in the first half of the waveform. A shear transformation is applied to the section from the minimum (of the first half of the waveform) to MX , and the minimum of the transformed section is found. The difference in these to time points indicates which is the true MN , as illustrated in Figures 6-7.

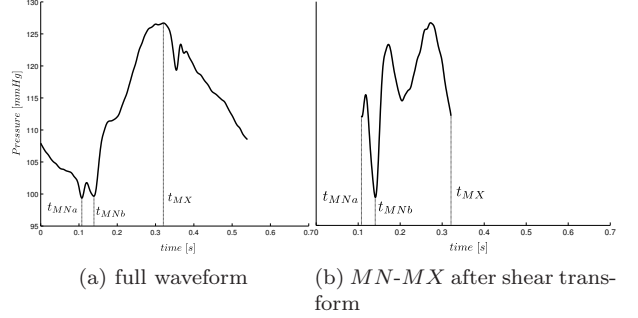


Fig. 6. An example where MN is not the global minimum

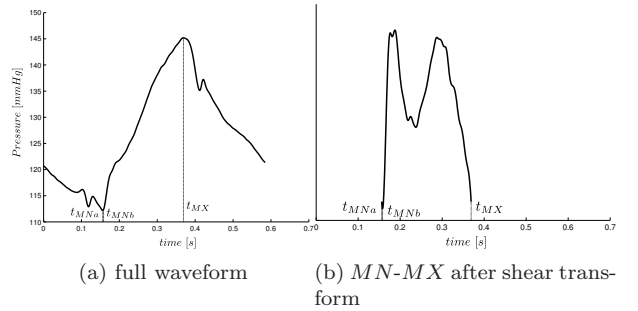


Fig. 7. An example where MN is the global minimum

First, locate the minimum of the first half of the waveform:

$$t_{MNa} \equiv \text{time of minimum of first half of } P_{ao} \quad (7)$$

Define the section between t_{MNa} and MX and pass it through the shear transformation of (3):

$$P_{ao,secA} \equiv \{P_{ao}(t) : t_{MNa} < t < t_{MX}\} \quad (8)$$

$$t_{MNb} \equiv \text{time of minimum } \phi_{shear}(P_{ao,secA}) \quad (9)$$

A threshold is then applied to the distance between t_{MNa} and t_{MNb} , to select the real MN , defined:

$$\text{error}_{P_{ao}} \equiv \frac{t_{MNb} - t_{MNa}}{\text{period}} \quad (10)$$

and

$$t_{MN} = t_{MNb}, \text{error}_{P_{ao}} < 0.025 \\ = t_{MNa}, \text{otherwise} \quad (11)$$

The constant 0.025 was found empirically, and the final value of t_{MN} in (11) gives good results in all cases.

Note that for P_{pa} , a shear transformation is not required as the case of Figure 6 never occurs. Thus, the method simply calculates:

$$t_{MN} \equiv \text{time of global minimum } P_{pa} \quad (12)$$

$DMPG$ is only needed for the P_{ao} waveform and is found by applying the shear transformation of (3) to a small

neighbourhood to the left of MN . The specific section, and condition are defined:

$$P_{ao,secB} \equiv \{P_{ao}(t) : \frac{3}{4} \cdot t_{MN} < t < t_{MN}\} \quad (13)$$

$$C_E \equiv (t_{MX} - t_{MN}) < period \cdot 0.23 \quad (14)$$

Where the both fraction $3/4$ and the constant 0.23 were empirically derived. The time t_{DMPG} is then defined:

$$t_{DMPG} \equiv \text{time of local maximum } \phi_{shear}(P_{ao,secB}) \quad (15)$$

To account for some waveforms that have an early rise (which is consistent with shorter pressure pulse) t_{DMPG} may be changed, as defined:

$$\begin{aligned} t_{DMPG} &\equiv t_{MN}, \text{ if } C_E \\ &\equiv t_{DMPG}, \text{ otherwise} \end{aligned} \quad (16)$$

3.3 LS and MPG

Both points LS and MPG are defined only for P_{ao} . MPG is one of the most important features physiologically and clinically, and is commonly called $dP_{ao}dt_{max}$, which is well known to relate to ventricle contractility.

To locate LS a new section is defined:

$$P_{ao,secC} \equiv \{P_{ao}(t) : t_{MN} < t < t_{MX}\} \quad (17)$$

The simplest approach to finding LS would be to locate the maximum of $\phi_{shear}(P_{ao,secC})$, as in Figure 5. However, in a number of cases, the shear transformation produces a second, higher peak. For example, for a curve shape like Figure 2, this second, higher peak would be the second ‘bump’ between MN and MX , which is the wrong point. The solution is to find both local maxima then have a second criteria to distinguish the correct point. The first maximum is:

$$t_{LSa} \equiv \text{time of maximum } \phi_{shear}(P_{ao,secC}) \quad (18)$$

To account for the case of t_{LSa} being the wrong point, which means it will be far up the waveform past LS , a section is defined:

$$P_{ao,secC2} \equiv \{P_{ao}(t) : t_{MN} < t < t_{LSa}\} \quad (19)$$

For this case, the correct time of LS should be:

$$t_{LSb} \equiv \text{time of maximum } \phi_{shear}(P_{ao,secC2}) \quad (20)$$

However, in a number of cases t_{LSa} is correct, which would mean t_{LSb} is a false point that lies somewhere between MN and LS in Figure 1. To account for both of these cases the solution is:

$$\begin{aligned} t_{LS} &= t_{LSa}, (t_{LSa} - t_{LSb}) < \frac{period}{20} \\ &= t_{LSb}, \text{ otherwise} \end{aligned} \quad (21)$$

where t_{LSa} and t_{LSb} are given by (18) and (20).

The first condition of (21) is due to the curve from MN to LS being close to sigmoidal so that when t_{LSa} is the correct point, t_{LSb} is always very close and within a 20th of the period. In the case where t_{LSa} is incorrect, and thus t_{LSb} is the correct point, $t_{LSa} - t_{LSb}$ is much greater than 20th of the period, and, in fact, is commonly between a 10th to a 5th of the period.

Once t_{LS} is found, the time point corresponding to MPG in Figure 1 is defined:

$$t_{MPG} \equiv \text{time of maximum } \left\{ \frac{d}{dt}(P_{ao}(t)) : t_{MN} < t < t_{LS} \right\} \quad (22)$$

3.4 DN, RS and DC

Note that RS and DC are only defined for P_{ao} .

The dicrotic notch (DN) in Figure 1 occurs at the close of the aortic valve, which corresponds to the end of ejection. The simplest way of defining t_{DN} would be to use t_{MX} from (6) and to compute the minimum of the shear transformed data for $t_{MX} < t < t_{end}$, where $t_{end} = period$. However, in a number of cases near the end of the trial, when the pig is near death, the maximum peak of P_{ao} occurs between the two points LS and MX in Figure 1. Physiologically this phenomenon is likely due to the twisting of the ventricle becoming abnormal and dysfunctional. In practice, it is probably too late to save a patient if this occurs. However, for completeness, this scenario is accounted for in the following method. Figure 8 shows an example of this case.

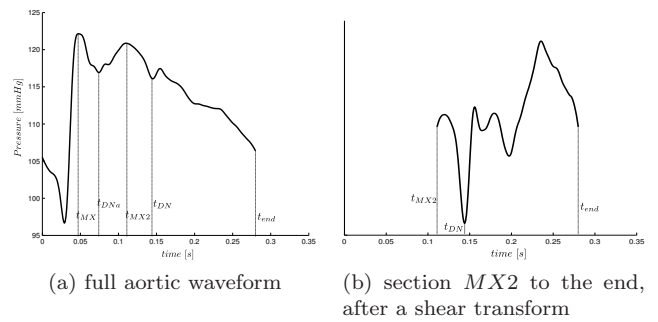


Fig. 8. An example where the MX needs to be moved to correctly locate DN

To ensure that the correct value of t_{MN} is obtained for the case of Figure 8, an estimate of the first local minima just after t_{MX} is empirically determined from all similar cases to Figure 8. The result is:

$$t_{DNa} \equiv t_{MN} + \frac{period}{5} \quad (23)$$

and this time point is shown in Figure 8a. There is some variation in the position of t_{DNa} , but, importantly it always occurs before the true dicrotic notch and after the first local minima following T_{MX} . A second estimate of DN is defined:

$$t_{DNb} \equiv \text{time of local minimum } DN_{shear} \quad (24)$$

where:

$$DN_{shear} \equiv \phi_{shear}(P_{ao,secD}) \quad (25)$$

$$P_{ao,secD} \equiv \{P_{ao}(t) : t_{MX2} < t < t_{end}\} \quad (26)$$

$$t_{MX2} \equiv \text{time of maximum } \{P_{ao}(t) : t_{DNa} < t < t_{end}\} \quad (27)$$

Note that DN_{shear} is smoothed using a ‘loess’ method over a 0.06 second range, this is to eliminate any fine oscillation in the waveform which would affect the location of t_{DNc} . There are a handful of cases where t_{DNa} still does not match the correct location for DN , due to a later, lower trough as in Figure 9. However it is not sufficient to just take the first local min of DN_{shear} as illustrated in Figure 10. To accommodate for these cases, a third possibility for DN is defined along with four conditions are defined to select between the first and lowest local minimum of DN_{shear} :

$$t_{DNc} \equiv \text{time of first local minimum of } DN_{shear} \quad (28)$$

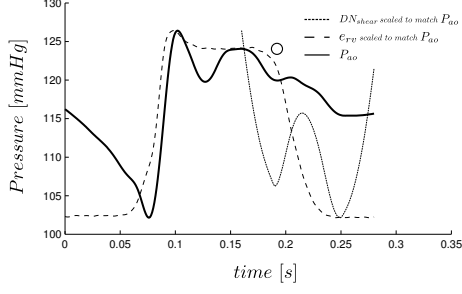


Fig. 9. An example of where the lowest local minimum of DN_{shear} does not match the real location for DN (shown with a circle). Note that the start and end of DN_{shear} are not the same due to heavy smoothing.

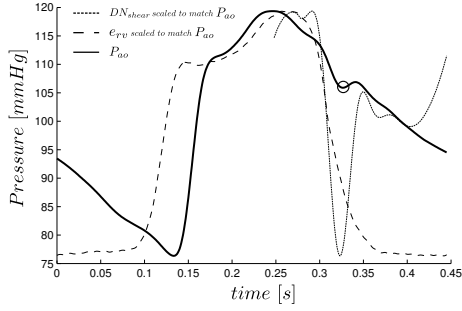


Fig. 10. In this case the lowest local min of DN_{shear} is the real DN (shown with a circle) but the first local min is not.

$$\begin{aligned}
 C_A &\equiv DN_{shear}(t_{DNc}) > DN_{shear}(t_{MX2}) \\
 C_B &\equiv (t_{DNc} - t_{MX2}) < 0.15 \cdot period \\
 C_C &\equiv \frac{DN_{shear}(t_{DNc}) - DN_{shear}(t_{DNb})}{P_{ao}(t_{MX})} > 0.02 \\
 C_D &\equiv t_{DNc} - t_{MX2} < 0.11 \cdot period
 \end{aligned} \quad (29)$$

The motivation behind these conditions are as follows: C_A prevents the choice of a local minimum, above the starting point of the transformed data, see Figure 10. However, this is only the wrong point if it occurs early, hence C_B and the use them together. C_C prevents the choice of a local minimum that is too much above the lowest local minimum, again this is only the wrong point if it occurs early, hence C_D and the use of C_C and C_D together.

From the conditions in (29), the final location for DN is defined:

$$\begin{aligned}
 t_{DN} &= t_{DNb}, \text{ if } (C_A \text{ AND } C_B) \text{ OR } (C_C \text{ AND } C_D) \\
 &= t_{DNc}, \text{ otherwise}
 \end{aligned} \quad (30)$$

For P_{pa} , the final value is simply:

$$t_{DN} = t_{DNb} \quad (31)$$

t_{DN} is then adjusted to the local minimum within a range of $period \cdot 0.04$ seconds, if such a minimum exists. This is necessary due to the fact that the minimum is located based on a sheared waveform and hence is slightly off the minimum of the true waveform.

The remaining values, RS and DC , are only defined for P_{ao} . The value of t_{RS} is defined:

$$t_{RS} \equiv \text{time of maximum } \phi_{shear}(P_{ao,secE}) \quad (32)$$

where:

$$P_{ao,secE} \equiv \{P_{ao}(t) : t_{MX} < t < t_{DN}\} \quad (33)$$

Finally, the last section is defined:

$$P_{ao,secF} \equiv \{P_{ao}(t) : t_{DN} < t < t_{DN} + 0.05\} \quad (34)$$

and the crest after the dicrotic notch is found by:

$$t_{DC} \equiv \text{time of maximum } P_{ao,secF} \quad (35)$$

3.5 Summary

A summary of the overall process for P_{ao} is defined:

- Step 1. find t_{MX} using (6)
- Step 2. find t_{MN} with (7)-(11) for P_{ao} or (12) for P_{pa}
- Step 3. find t_{DMPG} with (13)-(16)
- Step 4. find t_{LS} with (17)-(21)
- Step 5. find t_{MPG} between MN and LS , (22)
- Step 6. find t_{DN} with (23)-(30)
- Step 7. find t_{RS} with (32)-(33)
- Step 8. find t_{DC} using (34)-(35)

A summary of the overall process for P_{pa} is defined:

- Step 1. find t_{MX} using (6)
- Step 2. find t_{MN} with (7)-(11) for P_{ao} or (12) for P_{pa}
- Step 3. find t_{DN} with (23)-(24) and (31)

4. RESULTS

The method presented in this paper was developed on a set of five pigs (51 waveforms) that were induced with pulmonary embolism (Desaive et al. (2005); Ghuysen et al. (2008)), and further developed on another five pigs (37 waveforms) that were induced with septic shock (Lambertmont et al. (2003, 2006)).

The points for each waveform manually identified, after which the method was applied to the waveforms and assessed against the manually identified points. For the points (MN and DN) required in the pulmonary artery waveform, the method located both points in 87 of the 88 waveforms to within the sample frequency of 200Hz. The method only missed a single point, DN , from one waveform. This waveform was at the start of the third pig of the sepsis cohort and is unique to the data set, both in the driver function measured and the pulmonary artery pressure waveform, shown in Figure 11, see Figure 2 for a more normal P_{pa} waveform. The reason that the method failed to identify the correct location for DN is the unusual second peak of P_{pa} , and the early decay of the driver function.

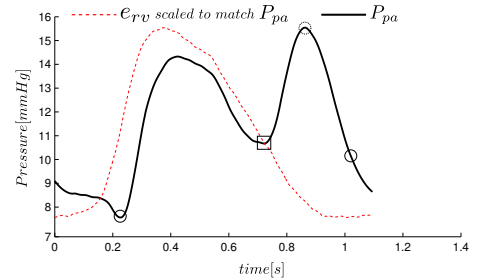


Fig. 11. Pulmonary artery waveform, alongside the matching driver function. The method failed to capture the correct DN in this case. The three circles are the identified points, from left to right MN , MX , DN . The real location for DN is marked by a square.

For each aortic pressure waveform, the method locates nine points. However, two of these, *RS* and *MN*, are only used in aiding the location of other points. Hence, the tolerance on their location is much larger than the other points. These two points were both located sufficiently to enable the method to progress in all 88 waveforms. Results for the other seven points are shown below in Table 2.

Table 2. Accuracy of the method: number of points grouped by accuracy of location

	< 1%	1 – 5%	5 – 10%	10 – 20%
<i>DMPG</i>	84	1	3	0
<i>MPG</i>	88	0	0	0
<i>LS</i>	86	1	1	0
<i>MX</i>	88	0	0	0
<i>MNG</i>	87	0	0	1
<i>DN</i>	86	2	0	0
<i>DC</i>	86	1	0	1
TOTAL	605	5	4	2

A similar method (for locating the points on the pressure waveforms) was used to estimate the driver functions (Stevenson et al. (2010)) which produced excellent results comparing, for pulmonary embolism, the approximated driver functions to the measured driver functions, see Table 3, and correlations with *R* values ranging from 0.81 to 0.99 for the left side and 0.73 to 0.98 for the right side. Using the same approach as (Stevenson et al. (2010)), the results for the driver functions for pulmonary embolism are also shown in Table 3.

Table 3. Errors in the reconstructed driver functions, from (Stevenson et al. (2010)), and this paper.

	Stevenson et al. (2010)		this paper	
	left	right	left	right
median	1.32%	2.50%	1.20%	2.50%
90 th percentile	3.67%	9.43%	3.55%	9.21%

5. DISCUSSION

The method detailed in this paper is useful primarily when combined with the mapping between aortic pressure, pulmonary artery pressure and the ventricle driver functions, (Stevenson et al. (2010)). Once combined, they provide a very useful tool, directly to clinicians, and indirectly via a previously developed cardiovascular model.

The method described in this paper worked well, however, not perfectly. The waveforms that the method has to handle can be quite different and hence it is very hard to achieve perfect results. The method was initially developed on just five pigs induced with pulmonary embolism, and afterwards adapted to also work with another set of five pigs induced with septic shock (with haemofiltration). The adaptations to make this possible, were few and small, demonstrating the robustness of the overall approach, and giving confidence that this method will generalize to a wider set of disease states, and to the human physiology as well.

Note that for this method a Swan-Ganz catheter is assumed, if radial artery pressure was measured instead, there would be more oscillations in the waveform, which would require modification of the method to handle them.

REFERENCES

- Desaive, T., Dutron, S., Lambermont, B., Kolh, P., Hann, C.E., Chase, J.G., Dauby, P.C., and Ghuysen, A. (2005). Close-loop model of the cardiovascular system including ventricular interaction and valve dynamics: application to pulmonary embolism. *12th Intl Conference on Biomedical Engineering (ICBME)*.
- Ghuysen, A., Lambermont, B., Kolh, P., Tchana-Sato, V., Magis, D., Gerard, P., Mommens, V., Janssen, N., Desaive, T., and D’Orio, V. (2008). Alteration of right ventricular-pulmonary vascular coupling in a porcine model of progressive pressure overloading. *Shock*, 29(2), 197–204.
- Grenvik, A., Ayres, S.M., and Holbrook, P.R. (1989). *Textbook of Critical Care*.
- Guyton, A. and Hall, J. (2000). *Textbook of Medical Physiology*.
- Lambermont, B., Delanaye, P., Dogne, J.M., Ghuysen, A., Janssen, N., Dubois, B., Desaive, T., Kolh, P., D’Orio, V., and Krzesinski, J.M. (2006). Large-pore membrane hemofiltration increases cytokine clearance and improves right ventricular-vascular coupling during endotoxic shock in pigs. *Artif Organs*, 30(7), 560–4.
- Lambermont, B., Ghuysen, A., Kolh, P., Tchana-Sato, V., Segers, P., Gerard, P., Morimont, P., Magis, D., Dogne, J.M., Masereel, B., and D’Orio, V. (2003). Effects of endotoxic shock on right ventricular systolic function and mechanical efficiency. *Cardiovasc Res*, 59(2), 412–8.
- Oommen, B., Karamanoglu, M., and Kovacs, S.J. (2003). Modeling time varying elastance: the meaning of “load-independence”. *Cardiovascular Engineering*, 3(4), 123–30.
- Senzaki, H., Chen, C.H., and Kass, D.A. (1996). Single-beat estimation of end-systolic pressure-volume relation in humans. A new method with the potential for noninvasive application. *Circulation*, 94(10), 2497–506.
- Smith, B.W., Chase, J.G., Nokes, R.I., Shaw, G.M., and Wake, G. (2004). Minimal haemodynamic system model including ventricular interaction and valve dynamics. *Med Eng Phys*, 26(2), 131–9.
- Starfinger, C., Chase, J.G., Hann, C.E., Shaw, G.M., Lambermont, B., Ghuysen, A., Kolh, P., Dauby, P.C., and Desaive, T. (2008). Model-based identification and diagnosis of a porcine model of induced endotoxic shock with hemofiltration. *Math Biosci*, 216(2), 132–9.
- Stevenson, D., Hann, C.E., Chase, J.G., Revie, J., Shaw, G.M., Desaive, T., Lambermont, B., Ghuysen, A., Kolh, P., and Heldmann, S. (2010). Estimating the driver function of a cardiovascular system model. *UKACC Intl Conference on Controls*.
- Suga, H. and Sagawa, K. (1974). Instantaneous pressure-volume relationships and their ratio in the excised, supported canine left ventricle. *Circ Res*, 35(1), 117–26.
- Suga, H., Sagawa, K., and Shoukas, A.A. (1973). Load independence of the instantaneous pressure-volume ratio of the canine left ventricle and effects of epinephrine and heart rate on the ratio. *Circ Res*, 32(3), 314–22.